



Lawrence Berkeley Laboratory

UNIVERSITY OF CALIFORNIA

Engineering Division

RECEIVED
LAWRENCE
BERKELEY LABORATORY

MAY 25 1988

LIBRARY AND
DOCUMENTS SECTION

Submitted to Applied Optics

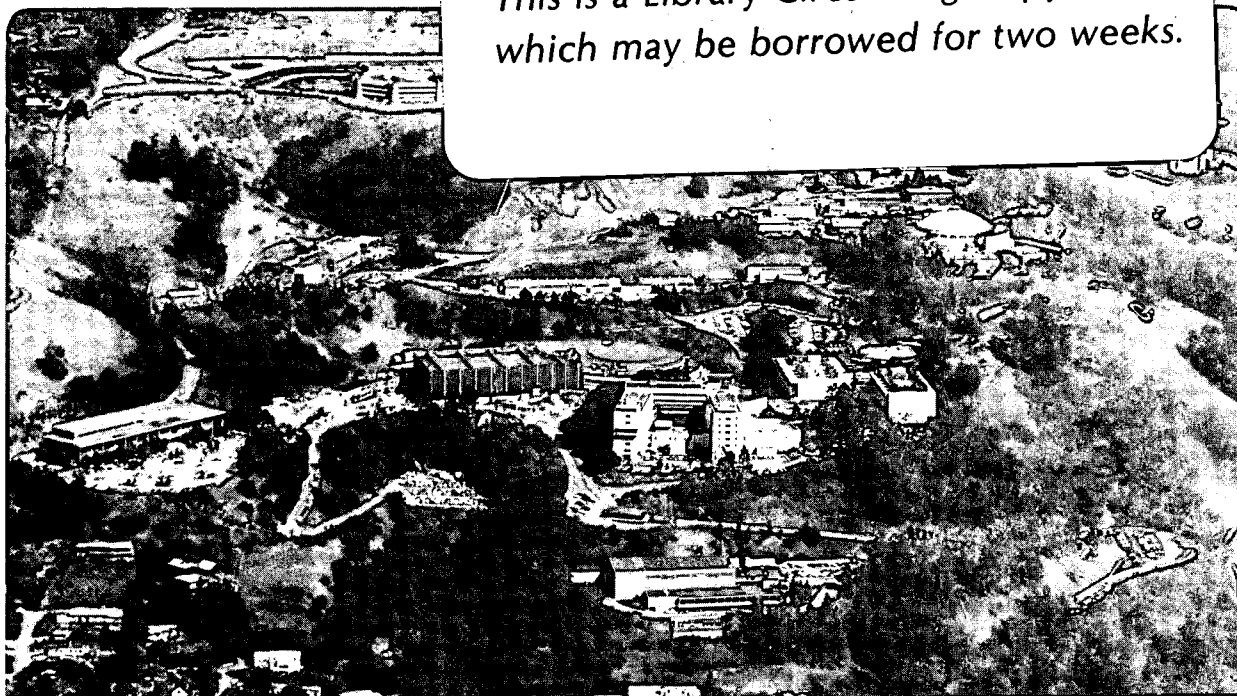
Germanium: Gallium Photoconductors for Far-Infrared Heterodyne Detection

I.S. Park, E.E. Haller,
E.N. Grossman, and D.M. Watson

February 1988

TWO-WEEK LOAN COPY

*This is a Library Circulating Copy
which may be borrowed for two weeks.*



DISCLAIMER

This document was prepared as an account of work sponsored by the United States Government. While this document is believed to contain correct information, neither the United States Government nor any agency thereof, nor the Regents of the University of California, nor any of their employees, makes any warranty, express or implied, or assumes any legal responsibility for the accuracy, completeness, or usefulness of any information, apparatus, product, or process disclosed, or represents that its use would not infringe privately owned rights. Reference herein to any specific commercial product, process, or service by its trade name, trademark, manufacturer, or otherwise, does not necessarily constitute or imply its endorsement, recommendation, or favoring by the United States Government or any agency thereof, or the Regents of the University of California. The views and opinions of authors expressed herein do not necessarily state or reflect those of the United States Government or any agency thereof or the Regents of the University of California.

Germanium:Gallium Photoconductors for Far-Infrared Heterodyne Detection

I. S. Park, E. E. Haller

University of California, Berkeley, Dept. of Materials Science and Mineral Engineering
and Lawrence Berkeley Laboratory

E. N. Grossman*, and Dan M. Watson**

California Institute of Technology, Dept. of Physics

Abstract

Highly compensated Ge:Ga photoconductors have been fabricated and evaluated for high bandwidth heterodyne detection. Bandwidths up to 60 MHz have been obtained, with corresponding current responsivity .01 A/W.

* current address : Univ. of Texas, Dept. of Astronomy

** R.A. Millikan fellow in physics, California Institute of Technology

1. Introduction

Extrinsic germanium photoconductors have long been the premier devices for high sensitivity direct detection in the 20 - 200 μm wavelength region^{1,2}. Quantum efficiencies over 40 % and noise equivalent powers (NEPs) of less than $10^{-16} \text{ W-Hz}^{-1/2}$ have been achieved. Although well characterized in terms of responsivity and direct detection NEP, the high speed (comparable to the inverse recombination time) properties of photoconductive detectors have not been studied in any detail. Recently, however, considerable interest has arisen among astronomers, plasma physicists, and others, in extending the techniques of high sensitivity millimeter and submillimeter heterodyne detection to the far-infrared^{3,4}. In response, we have performed an investigation of the suitability of extrinsic photoconductors as heterodyne mixers in this wavelength region. In particular, the dependence of detector bandwidth on the concentration of compensating impurities is a critical issue in the optimization of heterodyne performance, and has hitherto not been studied in any detail, for shallow impurities.

Extrinsic photoconductors are used in many applications as "square-law" devices : their signal current output is proportional to the radiation power input, i.e. to the square of the incident field amplitudes⁵. The signal can be mixed with a strong continuous wave (CW) local oscillator (LO) field at a nearby frequency, leading to new frequencies : the sum and difference of the signal and LO frequencies, ν_s and ν_{LO} respectively. The difference frequency, $\nu_{IF} = \nu_s - \nu_{LO}$, can be made arbitrarily low. The signal frequency can be downconverted into a frequency range in which low noise amplifiers are available.

If the detector bias and pre-amplifier circuitry is properly designed, then the system bandwidth will be limited by the extrinsic photoconductor free carrier recombination time, $\tau_r = \frac{1}{2\pi B}$, where B is the 3 db bandwidth. The amplitude of the detector's current response

is given by

$$i_{ph} = \frac{eP}{h\nu} \left[\frac{\eta G}{1 + (\omega\tau_r)^2} \right] \quad (1a)$$

where $\frac{eP}{h\nu}$ is the rate at which photons of frequency ν are incident on the detector, η is the responsive quantum efficiency, and G is the photoconductive gain⁶. The photoconductive gain, in turn, is given by

$$G = \frac{\tau_r}{\tau_{tr}} = \tau_r \left(\frac{\mu E_b}{l} \right) \quad (1b)$$

where τ_{tr} is the mean time for carriers to transit the interelectrode distance l , μ is the drift mobility and E_b the DC bias field on the detector. Thus, there are three fundamental material parameters that completely characterize such a detector, the mobility, the recombination time, and the quantum efficiency.

If, again, the contributions due to the pre-amplifier and external circuitry may be neglected, then the noise in the output signal is dominated by fluctuations in i_{ph} due to "generation-recombination" noise, the analogue of shot noise in a diode. These fluctuations are described by the relation² :

$$\langle i_{gr}^2 \rangle = \frac{4ei_{ph}G}{1 + (\omega\tau_r)^2} \cdot (A^2/Hz) \quad (2)$$

where G is the photoconductive gain. The DC (photo)current, i_{ph} , is dominated by the photocurrent due to background blackbody radiation in direct detection applications and by the photocurrent due to the local oscillator (LO) in heterodyne applications. If there is significant dark current, it also contributes shot-like noise.

Early experimental semiconductor characterization studies⁷ yielded some information on carrier recombination at low temperature, but were generally made under conditions quite different from those of heterodyne photomixer applications. More recent studies of high speed photoconductors^{8,9} were either concerned with response to pulsed radiation sources,

in which the carrier dynamics might conceivably be different than in CW applications, or only examined a very limited number of (n-type) samples.

A substantial body of theory exists on free carrier recombination cross-sections in germanium at low temperature. Recombination is an inelastic process, with most of the binding energy carried away by acoustic phonons. Because the impurity ionization energy is much greater than the energy of an acoustic phonon, $E_I \gg kT$, direct recombination into the ground state is a multi-phonon process, with a correspondingly very small cross-section. Therefore, the dominant process is capture into highly excited states followed by a cascade of single phonon emissions (and absorptions), as the carrier gradually "diffuses" into the ground state. Roughly speaking, there are two groups of theoretical work on the process of carrier recombination. The first was begun by the "giant trap" theory of Lax¹⁰, and has since been modified and revised by many authors. Ascarelli and Rodriguez¹¹ developed a quantum mechanical version, and Brown and Rodriguez¹² also incorporated the phonon polarization. The second, which takes a fundamentally different approach to the problem, has been pursued by several workers and has been comprehensively reviewed by Abakumov, Perel', and Yassievitch¹³ (APY).

The Lax theory and its modifications are very complicated. They all involve a summation over the impurity's excited states of $\sum_{n=2}^{\infty} \sigma_n \beta_n$, where β_n is the "sticking probability", the probability that an impurity in state n will eventually decay into the ground state rather than be ionized. The result of Lax's original treatment is

$$\sigma_r = \left\{ \frac{\pi}{9} \left[\ln \left(\frac{\gamma}{1.78 \delta} \right) + \frac{\delta}{\gamma} \right] \right\} \frac{1}{l_i} \left(\frac{e^2}{\epsilon kT} \right)^3 \left(\frac{m^* s^2}{kT} \right)^2 \quad (3)$$

where

$$\gamma \equiv \frac{kT}{m^* s^2}.$$

Here, s is the speed of sound, l_i is the mean free path for acoustic phonon scattering, and δ is a dimensionless upper cutoff to the integral for the binding energy, which must be solved for numerically in terms of γ . Specifically, Lax's theory, (using his quoted values for parameters such as s , m^* , etc.), predicts $\sigma_r = 1.3 \times 10^{-12}$ cm² at 4.2 K. The results of Brown and Rodriguez cannot be expressed in an analytic form, but their numerical solution predicts a somewhat lower value, $\sigma_r = 3.5 \times 10^{-13}$ cm².

Abakumov, Perel', and Yassievitch¹³ state that the Lax theory and its extensions are wrong. The basic difference between APY's theory and Lax's has to do with the sticking probability at large n . Lax's theory supposes that the first capture event takes place to a level which has binding energy of order kT , i.e. $n \sim 5$. APY contend, on the other hand, that at large n , σ_n increases faster than β_n decreases, and therefore that the dominant process is recombination through very highly excited states, with binding energy $\ll kT$. APY's treatment is based on the Pitaevskii method for treating recombination in gases. Their final result is the precise analogue of the Thompson cross-section for recombination of electrons onto hydrogen ions, rescaled to account for dielectric screening :

$$\sigma_r = \pi r_T^2 \left(\frac{r_T}{l_0} \right), \quad (4)$$

where

$$r_T = \frac{e^2}{\epsilon kT}$$

is the radius from a center at which a carrier's binding energy would be kT . Thus, it is the radius at which a captured carrier has, on average, an even chance of staying bound. The factor r_T/l_0 is the probability that the carrier will collide with an acoustic phonon while it is within a range r_T of the center. For a capture to occur, such a collision is necessary in order to carry off the excess energy. Here, l_0 is identified as the mean distance traversed by

a carrier in one energy relaxation time., i.e. $l_0 = v_T \tau_i$. It is independent of temperature, and is related to the inelastic mean free path by a factor $l_0/l_i = \frac{kT}{2m^*v_T}$. In short, APY's theory leads to

$$\sigma_r = \frac{4\pi}{3} \frac{1}{l_0} \left(\frac{e^2}{\epsilon kT} \right)^3 = \frac{1.1 \times 10^{-9}}{T_K^3} \text{ cm}^2 \quad (5)$$

where the numerical value assumes an energy relaxation length of $l_0 = 4.3 \times 10^{-3}$ cm (APY 1977). The factor of 4/3 arises from a geometric average over paths within r_T of the scattering center.

The Lax and APY theories differ by a factor of approximately $\left(\frac{m^*v_T^2}{kT} \right)^2$. The question of the appropriate speed of sound to use is somewhat problematical, but assuming it lies somewhere between the values given by Lax for the longitudinal and transverse speeds, then $.3K < \frac{m^*v_T^2}{k} < .8K$. APY adopt a value of .73 K. Thus, at 4.2 K, the recombination cross-sections predicted by the two theories differ by over an order of magnitude.

Finally, we note that both theories predict a very steep increase in the recombination cross-section, and therefore a steep increase in the bandwidth, as the temperature is reduced. The temperature which is relevant in this case is that which describes the width of the hole distribution function, T_h , which at sufficiently high bias fields, can exceed the temperature of the lattice. APY predict a T_h^{-3} dependence of the cross-section, and therefore a $T_h^{-5/2}$ dependence of the bandwidth. Lax's theory predicts T_h^{-4} for the cross-section at high temperatures ($\gamma/\delta \gg 1$) and T_h^{-3} at low temperatures, where the bracketed term in equation 3 is no longer a valid approximation. This corresponds to a bandwidth varying as $T_h^{-7/2}$ at high temperatures and $T_h^{-5/2}$ at low temperatures. Brown and Rodriguez's modification of the Lax theory predicts a somewhat gentler temperature dependence: $\sigma_r \sim T_h^{-3}$ at high T_h and $\sigma_r \sim T_h^{-2}$ at low temperature.

2. Material Preparation

Photoconductors were fabricated from a germanium single crystal which was phosphorus doped in the range 5×10^{13} to $1 \times 10^{15} \text{cm}^{-3}$. The concentration of compensating acceptors in the crystal was estimated to be $1 \times 10^{12} \text{cm}^{-3}$ as determined from variable temperature Hall effect measurements. Neutron transmutation doping (NTD) was used to add further dopants to several 1 mm thick wafers of this crystal. NTD of germanium produces Ga acceptors and As and Se donors by neutron capture of Ge isotopes followed by nuclear electron capture ($^{71}\text{Ge} \rightarrow ^{71}\text{Ga}$) or beta decay ($^{75}\text{Ge} \rightarrow ^{75}\text{As}$, $^{77}\text{Ge} \rightarrow ^{77}\text{As} \rightarrow ^{77}\text{Se}$), respectively¹⁴. The ratio of donors to acceptors created by NTD is given by isotopic abundance and neutron capture cross-sections. It leads to a compensation ratio of $(\text{As} + 2\text{Se}) / \text{Ga} = 0.32^{14}$. All concentrations of our samples are given in Table 1. As shown, we chose three neutron fluences leading to three series of samples, each having a specific concentration of Ga and varying concentrations of compensating donors. After NTD, the Ge wafers were annealed at 400° C for 6 hours in an Ar atmosphere to remove radiation damage caused mainly by fast neutrons, and to activate impurities¹⁵. Ohmic contacts were produced by implantation with boron ($1 \times 10^{14} \text{cm}^{-2}$ at 25 keV and $2 \times 10^{14} \text{cm}^{-2}$ at 50 keV). These implant doses lead to degenerately (i.e. metallicly) doped contact areas. 200 Å of Pd and 8000 Å of Au were then sputtered on the implanted surface. The final size of the detectors was $3.0 \times 1.0 \times 0.5 \text{mm}^3$ with electrodes on opposite $1 \times 3 \text{mm}^2$ surfaces.

3. Material Characterization

A complete characterization of the photoconductors would consist of a determination of the quantum efficiency as a function of wavelength, and determinations of the recombination

Table 1 – Doping Concentrations of Samples (cm^{-3})

Series	Sample	As grown (P)	NTD		Final	
			N_A	N_D	N_A	N_D
20	496-5.5(20)	$\sim 10^{12}$	3×10^{14}	9.6×10^{13}	3×10^{14}	9.6×10^{13}
	729-6.0(20)	5.0×10^{13}	3×10^{14}	9.6×10^{13}	3×10^{14}	1.4×10^{14}
	729-9.0(20)	8.0×10^{13}	3×10^{14}	9.6×10^{13}	3×10^{14}	1.8×10^{14}
	729-13.0(20)	1.0×10^{14}	3×10^{14}	9.6×10^{13}	3×10^{14}	2.0×10^{14}
21	729-6.4(21)	5.0×10^{13}	6×10^{14}	1.9×10^{14}	6×10^{14}	2.4×10^{14}
	729-9.4(21)	8.0×10^{13}	6×10^{14}	1.9×10^{14}	6×10^{14}	2.7×10^{14}
	729-14.6(21)	1.5×10^{14}	6×10^{14}	1.9×10^{14}	6×10^{14}	3.4×10^{14}
22	729-6.4(22)	5.0×10^{13}	1×10^{15}	3.2×10^{14}	1×10^{15}	3.7×10^{14}
	729-9.4(22)	8.0×10^{13}	1×10^{15}	3.2×10^{14}	1×10^{15}	4.0×10^{14}
	729-14.6(22)	1.5×10^{14}	1×10^{15}	3.2×10^{14}	1×10^{15}	4.7×10^{14}
	729-17.0(22)	2.0×10^{14}	1×10^{15}	3.2×10^{14}	1×10^{15}	5.2×10^{14}

time and mobility as functions of bias field. These three material parameters are related to three directly observable detector properties, namely the wavelength-dependent responsivity, (defined from equation 1a as i_{ph}/P), the bandwidth, and the photoconductive gain, via equations 1a-1b. For each detector characterized, we have determined the low field mobility by variable-temperature Hall effect measurements, the direct-detection responsivity at $93 \mu\text{m}$ and $119 \mu\text{m}$, the bandwidth, as measured both by the frequency rolloff of g-r noise and by the frequency rolloff of response to directly modulated FIR radiation, and the photoconductive gain, as measured by the amplitude of the g-r noise. The systematic errors inherent in our experimental setup affect the accuracy of these different measurements to varying degrees, however. The nature of these systematic errors, and comparison between different sets

of partially redundant measurements indicate that our determinations of bandwidth are consistent and unambiguous, but that, for certain detectors, there are large discrepancies in the photoconductive gain (and therefore quantum efficiency) obtained by different methods.

The carrier mobility at 4.2 K was determined by variable-temperature Hall effect measurements performed on separate samples cut from the same wafers as the detectors used in the other measurements. Van der Pauw geometry was used with a sample size of $7 \times 7 \times 1 \text{ mm}^3$. Ohmic contacts were prepared by boron implantation on the four corners of the sample. Because of significant hopping (dark) conductivity at the high acceptor concentrations, Hall effect measurements could not be used to determine the drift mobility in the most heavily doped samples, namely the series 22 detectors.

Current responsivity was measured in direct (incoherent) detection at a wavelength of $93 \text{ }\mu\text{m}$ (near the peak of the unstressed Ge:Ga photoconductive response) by means of a series of liquid-helium temperature filters, including a narrow-bandwidth, Fabry-Perot filter. The voltage-biased detector was mounted in a conventional, cylindrical, integrating cavity and illuminated through the cold filters by radiation from a 300 K blackbody chopped at 20 Hz against a 77 K blackbody. The total power incident on the detectors was estimated to be approximately 10^{-13} W , or $\sim 5 \times 10^7 \text{ photon/s}$. The test system, filters, and procedures have been described previously¹⁶. All of our detectors produced measurable amounts of dark current. For the most heavily doped (series 22) detectors, the dark current, typically several nanoamps depending on the precise detector and bias voltage used, was consistent with that theoretically predicted¹⁷ for hopping conduction at the applicable acceptor and donor concentrations. Furthermore, for these detectors, it was sufficiently large that the dark current shot noise was larger than the signal current due to the $\sim 10^{-13} \text{ W}$ of incident blackbody radiation. To increase the photon flux, the direct-detection responsivity was

measured with the narrowband Fabry-Perot removed. The spectrum of incident radiation was now limited at long wavelengths only by the Ge:Ga photoconduction edge and at short wavelengths by the cutoff of the cold low-pass filters. This increased the flux of incident photons by a factor of 30, as measured by the photocurrent in detector # 729-6.0(20), which was used for the relative calibration. Because the setup is less well characterized in this configuration, and because of possible changes in the effective wavelength in this broadband mode, the 93 μm responsivities derived for the three 22-series detectors are considerably more uncertain than those of the other detectors.

The current responsivity measurements at 119 μm were made using the FIR laser described below that was used in the bandwidth and photoconductive gain measurements. The detectors were mounted at 4.2 K in similar integrating cavities of somewhat different dimensions than in the 93 μm measurements. The laser was operated on the strong 118.84 μm methanol line for all of our measurements. The laser beam was focussed on the input aperture of the cavity, and illuminated the detector through liquid-helium temperature low-pass filters. Current-voltage curves were recorded for each detector with the laser on, laser off, and (usually) laser attenuated by various amounts, as part of the setup procedure for the g-r noise measurements. The laser power was monitored from time to time by replacing the photoconductor with a pyroelectric detector. Linearity was checked by inserting attenuators into the laser beam and comparing the drop in detector photocurrent with that in the pyroelectric signal. There is a large (factor of 4) uncertainty in the absolute calibration of the pyroelectric detector which is reflected in the absolute 119 μm responsivities derived. The uncertainty in relative responsivities, however, is limited only by laser power drifts, and is much better, probably, $\pm 25\%$. Comparison of the relative 119 μm responsivities with other data is difficult, however, because the 119 μm laser wavelength lies on the photocon-

ductivity edge of Ge:Ga, whose width increases markedly with acceptor concentration due to wavefunction overlap. Thus, the quantum efficiency is likely to vary from detector to detector much more at 119 μm than at 93 μm .

Photoconductive gain and recombination bandwidth for each detector were measured with the use of a FIR heterodyne receiver, illustrated in Figure 1 and described in detail elsewhere^{18,19}. Briefly, the system consists of a photoconductor, an 80 μm lowpass filter, and a low-noise 1-100 MHz GaAsFET amplifier mounted in a liquid helium dewar. Ordinarily, a FIR laser sideband generator provides a continuously tunable local oscillator for the receiver. Two techniques were used to measure detector bandwidths. The more direct one consisted of amplitude modulation of the beam of the optically-pumped FIR molecular laser and measurement of the rolloff in modulated photocurrent as the modulation frequency was swept. A reflective FIR modulator was implemented by modifying the laser sideband generator shown in Figure 1. The heart of the sideband generator is an ultra-low capacitance Schottky diode (batch no. 1E12, obtained from R. Mattauch's group at the Univ. of Virginia) at the feed of a traveling-wave corner-cube antenna²⁰ which couples it to the incident laser beam. Modulation occurs because the traveling wave induced on the antenna is reflected off the impedance mismatch presented by the Schottky diode and re-radiated. The reflection coefficient depends on the (modulated) Schottky bias voltage. Thus, for our bandwidth measurements, the 2-18 GHz YIG oscillators were replaced with a 5-100 MHz voltage-controlled oscillator (VCO), the polarizing Michelson interferometer was tuned to zero path difference, and the Fabry-Perot interferometer removed. The same voltage ramp that was used to drive the VCO was also used to drive the internal VCO of a spectrum analyzer with which the amplified detector photocurrent measured. Because the two VCO's were not precisely matched in linearity, the peak spectrum analyzer response would gradu-

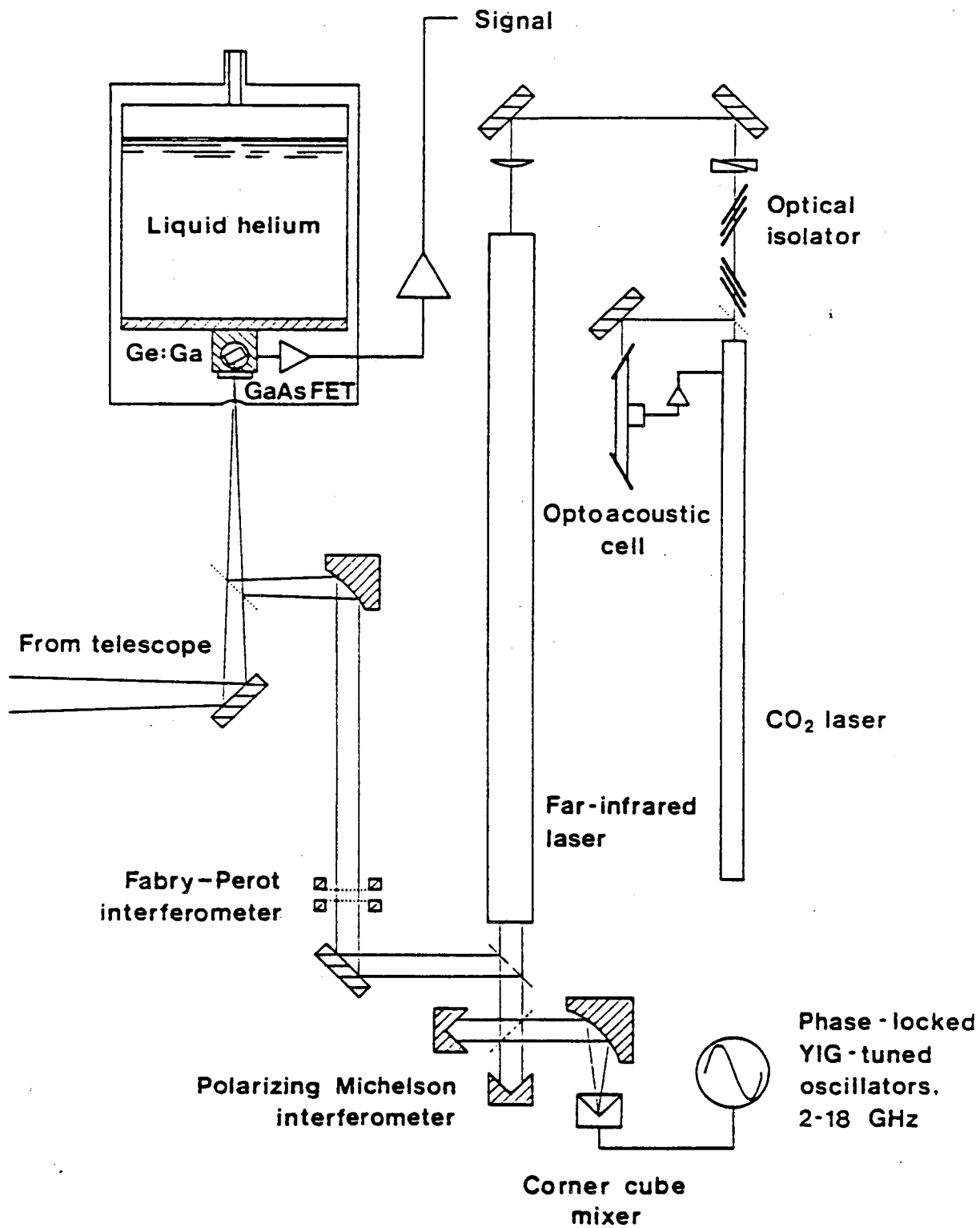


Figure 1 - Block diagram the FIR heterodyne receiver used, in modified form, to measure Ge:Ga bandwidth and photoconductive gain (Watson, Grossman, and Phillips 1988)

XBL 882-585

ally drift away from the actual modulation frequency as the two were scanned, limiting the useful length of a single sweep to ~ 45 MHz. Because the depth of modulation of the FIR laser beam was very low, due to the Schottky diode parasitics²¹, the broadband amplifier noise was not completely negligible, particularly for the high-bandwidth, low-gain detectors. Therefore, a spectrum analyzer scan with the laser blocked was recorded immediately before each data scan. The digitized scans were subtracted and the difference fitted to the Lorentzian spectrum of equation 1a.

The second technique for measuring recombination bandwidth consisted of measurement of the spectrum of the photocurrent's g-r noise. The corner-cube modulator and polarizing Michelson interferometer were removed and the FIR laser focussed directly onto the detector cavity's entrance aperture. Spectra of the amplified photocurrent power spectrum with the laser on, laser attenuated by various amounts, and laser blocked, were recorded and digitized. The conversion from noise power spectral density at the amplifier output (what the spectrum analyzer measures) and RMS photocurrent is given by

$$P_{out}/B = A \left(\frac{R_d R_a}{R_d + R_a} \right) (i^2) \quad (W/Hz) \quad (6)$$

where A is the power gain of the amplifiers, B the resolution bandwidth of the spectrum analyzer, R_a the input impedance of the first stage pre-amplifier, and R_d the differential impedance of the detector. The single-stage, cryogenic GaAsFET per-amplifier used in these measurements intrinsically has a very high input impedance. In order to improve the gain flatness, the flatness of the noise spectrum, and the system stability, its input, i.e. the IF signal line, is shunted by a resistor. When optimum noise performance is desired, the value of the resistor (which determines R_a) is roughly matched to R_d . For our measurements, however, the value of the resistor was set much lower, generally 200Ω , in order that RC rolloff due to amplifier input capacitance and to parasitic capacitance would

not contaminate the detector's intrinsic rolloff. Again, a spectrum taken with the laser blocked was subtracted from each data scan and the difference fitted to a Lorentzian. As given by equation 2, the rolloff frequency yielded the carrier lifetime and the overall power, divided by the DC photocurrent, yielded the photoconductive gain.

There are two significant sources of uncertainty in this measurement. The simplest is merely the calibration of amplifier and spectrum analyzer gains. We estimate that these uncertainties could total as much as 3 db. They are only relevant to the determination of the photoconductive gain, of course, and not to the determination of the bandwidth. The other source of uncertainty is the sporadic existence of low-frequency (< 10 MHz) noise on the laser. If it was discovered in real time, it was always found to be possible to retune the laser so as to eliminate the noise, albeit with some sacrifice in laser power. In about one third of the measured spectra, however, an additional low-frequency component (taken to be another Lorentzian) was required in order to obtain an acceptable fit. In all such cases, there were spectra taken at three or more power levels so that it was possible to confirm that the excess noise component varied quadratically with laser power, as expected for laser noise. The remaining noise did fit a single Lorentzian spectrum, and scaled linearly with laser power, so we are confident it was indeed detector g-r noise. The recombination bandwidths determined by this technique agree very well with those derived by the modulation technique. The excess noise subtraction does introduce additional uncertainty into the determination of photoconductive gain (and therefore quantum efficiency) in those cases for which it was necessary. Together with the uncertainty introduced by the gain calibration, this renders our derived photoconductive gains considerably less reliable than our derived bandwidths.

4. Results and Discussion

Figure 2 shows our measurements of modulation bandwidth versus bias field for a single detector, # 496-5.5. The indicated error bars are somewhat conservative estimates of the range over which a good fit of the data to a single Lorentzian could be obtained. The falloff in bandwidth at high bias is due to the reduction in recombination cross-section that occurs as the carrier temperature T_h , is elevated above the lattice temperature.

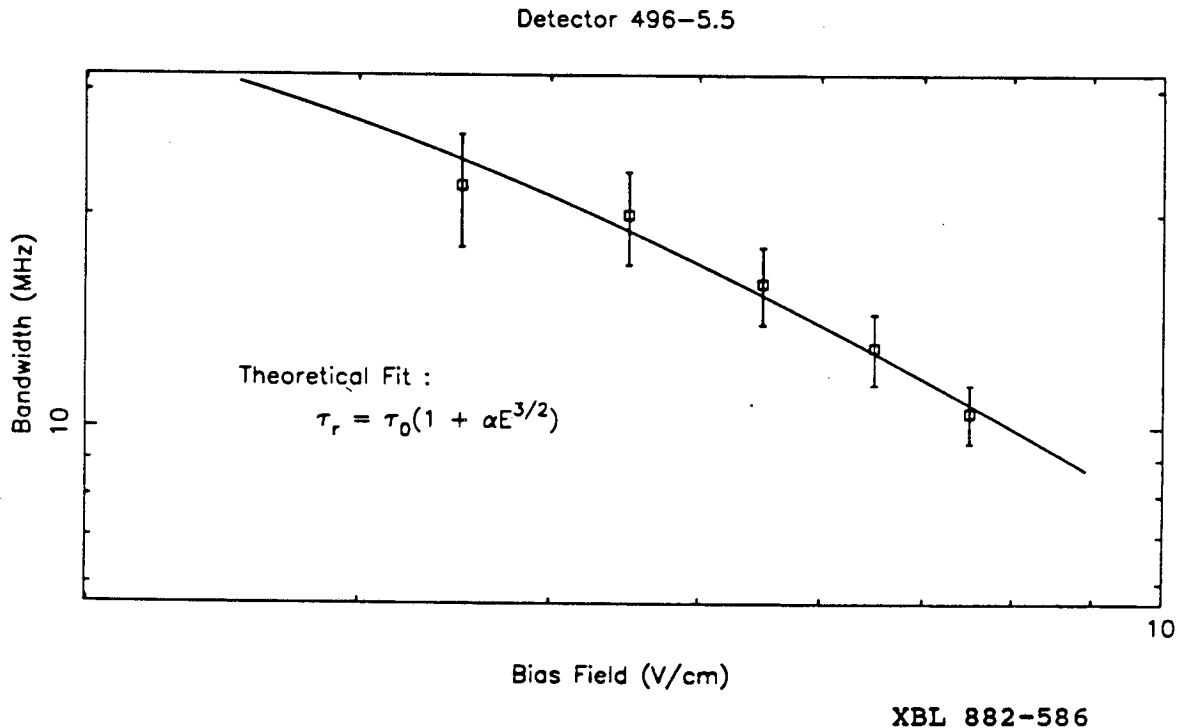


Figure 2 - Field dependence of the recombination bandwidth, measured on detector 496-5.5. The rolloff at high field is due to carrier heating.

A crude theoretical argument leads to the expectation that recombination bandwidth should vary as $B \propto E^{-3/2}$ in the hot carrier regime and be independent of E in the thermalized regime. According to the original "giant trap" theory of Lax, the recombination

cross-section varies with mean carrier kinetic energy U as $\sigma_r \propto U^{-2} \propto T_h^{-2} \propto v_T^{-4}$, (v_T is the total mean carrier velocity). Thus, the recombination bandwidth is expected to vary as

$$B = N_D \sigma_r v_T \propto N_D T_h^{-3/2} \quad (7)$$

where $N_D = N_A$ is the concentration of ionized acceptors. In the thermalized (low bias) regime, T_h is equal to the lattice temperature, independent of field. In the hot carrier regime, the relation between v_T and bias field is given⁶ by equating the rate at which energy is imparted to the carriers by the bias field with the rate at which energy is lost via inelastic (i.e. acoustic phonon) collisions. Thus,

$$eE v_d = \left(\frac{1}{2} m^* v_T^2 \right) \left(\frac{v_T}{l_i} \right), \quad (8)$$

where l_i is the inelastic mean free path. The drift velocity, v_d , is limited by ionized impurity scattering (an elastic process) and is $\ll v_T$. It is given by the acceleration due to the field over an elastic scattering time :

$$v_d = \frac{eE}{m^*} \left(\frac{l_e}{v_T} \right). \quad (9)$$

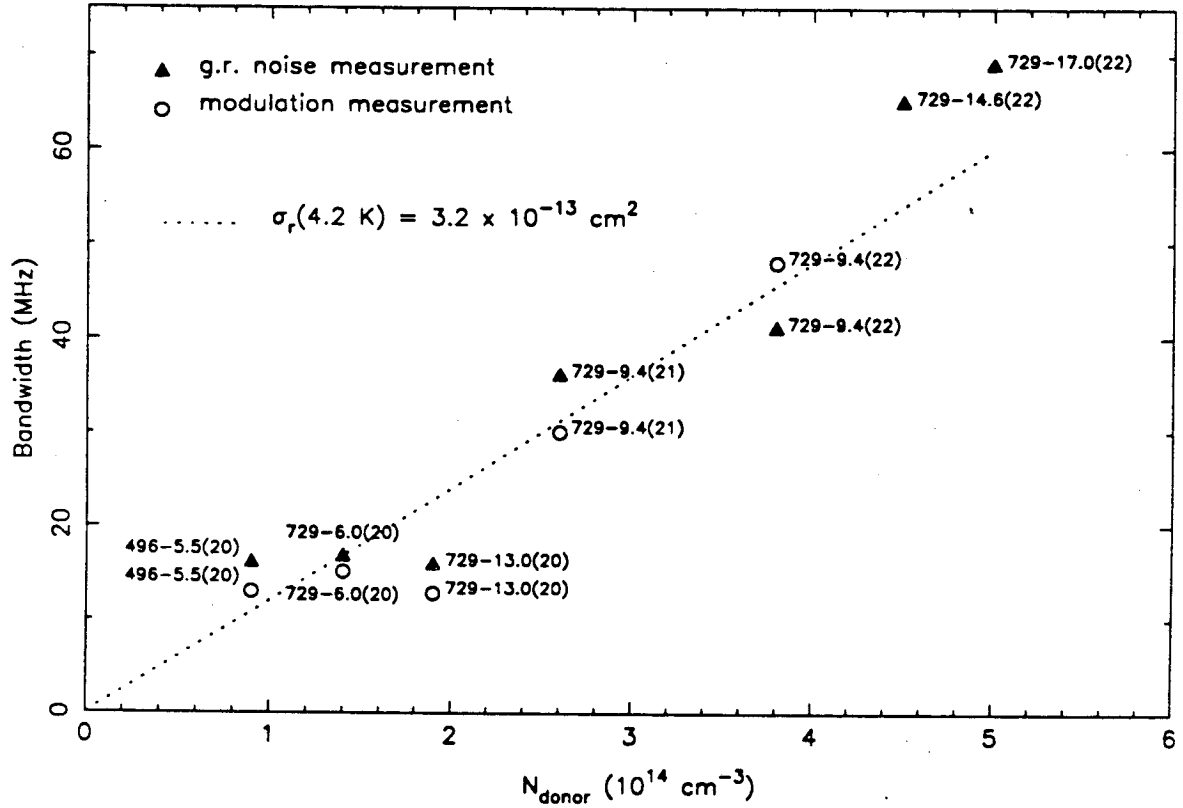
Combining (8) and (9), one finds $v_T \propto E^{1/2}$, or $T_h \propto E$. Thus, from equation 7, the theoretical expectation is thus that $B \propto E^{-3/2}$ in the hot carrier regime, and is independent of E in the thermalized regime.

As shown in Figure 2, such a dependence fits our data very well. Koenig, Brown, and Schillinger found for much less heavily doped, n-type germanium samples, ($N_d \sim 10^{13} \text{ cm}^{-3}$), that $B \propto E^{-1.8}$ in the hot carrier regime and was independent of E in the thermalized regime. Their lifetime measurements were made with a pulse technique, however, in which the detector slewed between conditions of impact-ionization breakdown and sub-breakdown bias (the normal operating condition,) at high speed. It has since been discovered that the

dynamic behaviour of the detectors becomes very complex near breakdown, often exhibiting high-speed spontaneous instabilities, period doubling, chaotic fluctuations, etc.²². Thus, the results of the pulsed measurements, taken in isolation, would be ambiguous. Although our measurements are in excellent agreement with the theoretical expectation deduced from equations 8 and 9, they are not sufficiently accurate, nor do they extend over a large enough range in bias, for us to test the dependence in great detail. We cannot distinguish between an $E^{-1.5}$ and an $E^{-1.8}$ dependence in the high bias limit, for example. Indeed, considering all the uncertainties, a bandwidth varying inversely with field is also an acceptable empirical approximation to our data over the range of practical interest, $.5E_b < E < E_b$.

One of the main reasons for our wanting to determine the dependence of bandwidth on bias is to be able to normalize $B(N_D)$, the bandwidth versus compensating impurity concentration, to a single value of E/E_{br} . Physically, the bandwidth in the low-bias limit, where the carriers are thermalized, would be the most fundamental quantity to examine. However, the low-bias limit is not the regime in which the photoconductors are used in practical applications, nor is it a region in which we can, with our techniques, measure the bandwidth with any accuracy. (In both cases, the responsivity is too low.) Therefore, we have normalized all our bandwidth measurements to a bias $E = 0.8E_{br}$ using the empirical approximation of $B \propto E^{-1}$ described above. The bandwidths were actually measured at biases that varied from about .7 to .95 times the breakdown field, so this normalization never amounted to more than about a 15 % correction. The results of our measurements, using both the modulation and the g.r. noise techniques, are displayed in Figure 3.

These bandwidth measurements are the central result of this work. It is clear that the two techniques employed to measure the bandwidth agree fairly well. The series 22 detectors have the highest bandwidths of any we have measured - some 60 MHz measured directly,



XBL 882-587

Figure 3 - Measured recombination bandwidth as a function of minority impurity concentration, for the NTD detectors. The dotted line corresponds to the linear dependence of equation 10, using a carrier temperature of $T_h = 4.2 \text{ K}$, and a recombination cross-section of $\sigma_r = 3.2 \times 10^{-13} \text{ cm}^2$.

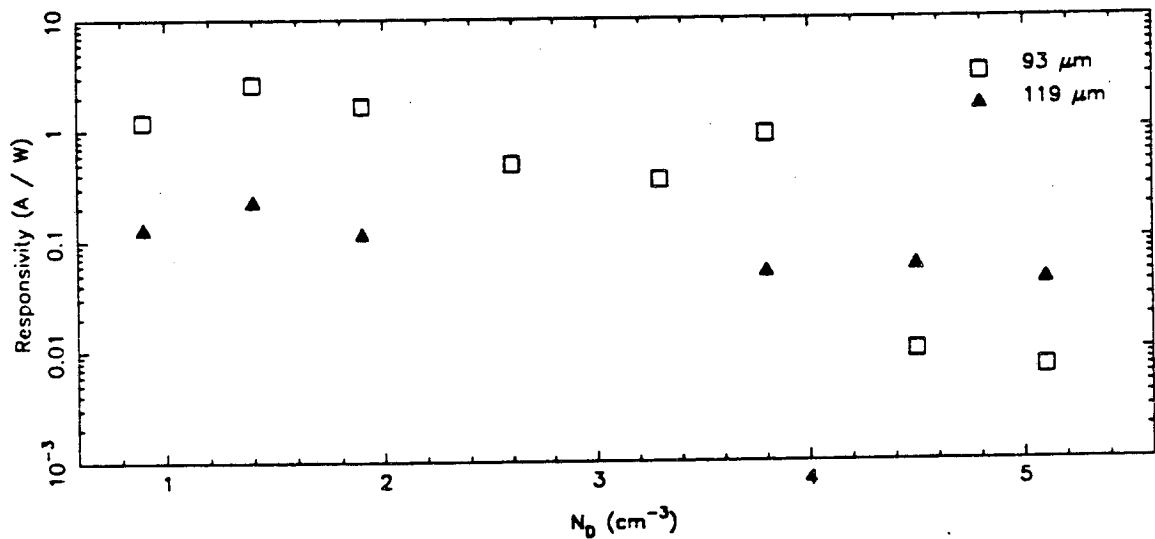
corresponding to 65 - 70 MHz at 0.8 times the breakdown field. As expected from equation 7, there is an approximately linear relation between bandwidth and donor concentration. The slope of the relation is a measure of the recombination cross-section via

$$\sigma_r = \frac{B(N_D)}{N_D v_T} = \frac{B(N_D)}{N_D} \left(\frac{3kT_h}{m^*} \right)^{-1/2} \quad (10)$$

Taking $T_h = 4.2K$ we obtain $\sigma_r = 3.2 \times 10^{-13} \text{ cm}^2$. This is a slight overestimate of the cross-section at the true carrier temperature (because of the $T_h^{-1/2}$ conversion factor in equation 10) but an underestimate of the cross-section at 4.2 K (because of the steep falloff of cross-section with temperature mentioned in section 1). Based on the measured bias dependence of bandwidth in Figure 2, we do not expect the bandwidth, and therefore σ_r , in the thermalized regime (i.e. at 4.2 K) to be more than perhaps a factor of two greater than our present determination, however. Comparing with the theories discussed earlier, it is clear that our data favor the Brown and Rodriguez result. However, to be fair, we note that since we do not know for certain the true carrier temperature in our experiments, the extremely steep dependence of σ_r on temperature may be used to make any of the theories fit the measured cross-section. For APY's theory, a carrier temperature of $T_h = 15K$ would have to be assumed (taking $\sigma_r \sim T_h^{-3}$), which seems implausibly high. For Lax's theory, $T_h = 5.8K$ (taking $\sigma_r \sim T_h^{-4}$) would suffice.

Figure 4 displays our 93 μm and 119 μm responsivity measurements. The plotted values were measured at slightly different biases from 0.7 to 0.9 times the breakdown field of the various respective detectors. The 93 μm measurements show a steep falloff in responsivity as N_d is increased. If η is approximately the same for all detectors at 93 μm (since this is well shortward of the photoconductive edge in germanium), then this falloff reflects the decline in photoconductive gain at high compensating impurity concentration. Such a decline is expected, partly due to the reduced recombination lifetime, and partly due to increased ionized impurity scattering and therefore reduced drift mobility. Our measured Hall mobilities indeed show such a decline, falling from $2.5 \times 10^4 \text{ cm}^2/\text{s}$ for detector 729-6.0(20) to $3000 \text{ cm}^2/\text{s}$ for 729-14.6(21). The 119 μm responsivities also show a falloff at high dopings, but it is not nearly such a steep one as that of the 93 μm responsivities. This may be

understood in terms of impurity wavefunction overlap at high dopings, whose existence is implied by the existence of significant dark currents. Evidently, as the doping level is raised, the photoconductive gain falls off as indicated by the 93 μm responsivity, but an increase in quantum efficiency due to broadening of the photoconductive edge partially compensates for this, so that the falloff in 119 μm responsivity is not so steep. As mentioned earlier, the absolute value of the 119 μm responsivity is somewhat uncertain due to the pyroelectric detector's absolute calibration. The fact that some of our measurements apparently indicate $S(93\mu\text{m}) > S(119\mu\text{m})$ does not therefore affect this interpretation.



XBL 882-588

Figure 4 - Direct detection responsivity as a function of compensating impurity concentration.

The photoconductive gains we have derived from the amplitude of the g-r noise are shown in Table 2. As discussed earlier, they are subject to significant uncertainties that do not affect our other data. The typical values, in the range of .01 - .03, are more than an order of magnitude lower than for typical detectors optimized for direct detection. In

addition, there is a decline in measured photoconductive gain with increasing N_D , but it is not nearly as fast as that of the 93 μm responsivity, which, as discussed above, should track G . Indeed, the rolloff in the measured G is, at the level of uncertainty in the data, no faster than that of $S(119\mu\text{m})$. This discrepancy in the rate at which G and $S(93\mu\text{m})$ decline with N_D is the basic inconsistency between our different sets of data. It depends heavily on the measured 93 μm responsivities of the two most highly doped (22-series) detectors, however. As discussed earlier, these are more uncertain than the other 93 μm responsivities because they were measured in a more poorly characterized configuration, without the Fabry-Perot narrowband filter. In sum, although there is clearly a rolloff in photoconductive gain, and therefore in responsivity, with increasing concentration of compensating impurities, our data are ambiguous regarding how fast the rolloff is.

Table 2 - Photoconductive gain derived from g-r noise

Sample	E_{bias} (V/cm)	μ_{Hall} ($\text{cm}^2/\text{V} - \text{s}$)	$G = \langle i^2 \rangle / 4ei_{DC}$
496-5.5(20)	5.5	-	.021
729-6.0(20)	9.8	2.5×10^4	.032
729-13.0(20)	15	9000	.028
729-9.4(21)	12	6000	.025
729-9.4(22)	18	-	.022
729-14.6(22)	20	-	.015
729-17.0(22)	25	-	.014

5. Conclusions

Ge:Ga photoconductive mixers have been developed for FIR heterodyne applications,

and recombination bandwidths as high as 60 MHz have been directly measured. The dependence of bandwidth on bias field is consistent with previous measurements of very lightly doped n-type material, and with theoretical expectations for the recombination cross-section in the hot-carrier regime. At a given fraction of breakdown voltage (corresponding in practice to a normal operating point) mixer bandwidth varies approximately linearly with the concentration of compensating donors. The slope of the relation yields a recombination cross-section of $\sigma_r = 3.2 \times 10^{-13} \left(\frac{4.2K}{T_h} \right)^{1/2} \text{ cm}^2$. This is close to the value predicted by Brown and Rodriguez's extension of Lax's giant-trap theory for thermalized carriers at 4.2 K, and about a factor of 30 smaller than the value predicted by APY. There is a marked rolloff in photoconductive gain at higher impurity concentrations.

These results indicate that Ge:Ga mixers can be fabricated with relatively large bandwidths. The increased bandwidth is obtained at the expense of photoconductive gain and responsivity, however. In heterodyne applications, the LO power required in order to obtain quantum noise limited performance (i.e. LO-induced g-r noise greater than other instrumental sources of noise) increases with the square of photoconductive gain. Thus, increased bandwidth is obtained at the price of greater – possibly much greater – required LO power. Optimization of a heterodyne system thus involves a compromise between desired bandwidth and available LO power.

Acknowledgments

We thank Dr. J. Farmer of the University of Missouri for neutron irradiation of germanium samples. Professor C. Townes has stimulated and contributed to this work in the early stages through numerous discussions and suggestions. This work was supported in part by NASA Contract No. W-14606 under Interagency Agreement with the Director's Office of Energy Research, Office of Health and Environmental Research, U.S. Department of En-

ergy under Contract No. DE-ACO3-76SF00098. Far-infrared heterodyne instrumentation research at Caltech is supported by NASA Grant NAGW107.

References

1. E.E. Haller , "Physics and Design of Advanced IR Bolometers and Photoconductors", *Infrared Physics*, **25**, 257 (1985).
- 2 . P.R. Bratt, Impurity Germanium and Silicon Infrared Detectors, chap. 2 in *Semiconductors and Semimetals* vol. 12, R.K. Willardson and C.A. Beer, ed., Academic Press, New York, 1977
- 3 . A.L. Betz and J. Zmuidzinas, in presentation to L. Fisk on SOFIA, (Stratospheric Observatory for Infrared Astronomy), Ames Research Center, 1987
4. H.P. Röser, R. Wattenbach, E.J. Durwen, and G.V. Schultz , "A High Resolution Heterodyne Spectrometer from $100\mu\text{m}$ to $1,000\mu\text{m}$ and the Detection of CO (J=7-6), CO (J=6-5), and CO (J=3-2)", *Astronomy and Astrophysics*, **165**, 287 (1986).
- 5 . P.L. Richards and L.T. Greenberg, in *Infrared and Millimeter Waves* vol. 6, Academic Press, New York, 1982
6. R.M. Westervelt and S.W. Teitsworth , "Nonlinear Transient Response of Extrinsic Ge Far-infrared Photoconductors", *J. Appl. Phys.*, **57**(12), 5457 (1985).
7. S.H. Koenig, R.D. Brown, and W. Schillinger (KBS) , "Electrical Conduction in n-Type Germanium at Low Temperatures", *Phys. Rev.*, **128**(4), 1668 (1962).
8. F. Kohl, W. Müller, and E. Gornik , "Speed Limitation of Ge Far-infrared Photoconductive Detectors", *Infrared Physics*, **18**, 697 (1978).
9. G. Dodel, J. Heppner, E. Holzhauser, and E. Gornik , "Wideband Heterodyne Detection in the Far-infrared with Extrinsic Ge Photoconductors", *J. Appl. Phys.*, **54**(8), 4254 (1983).
10. M. Lax , "Cascade Capture of Electrons in Solids", *Phys. Rev.*, **119**(5), 1502 (1960).
11. G. Ascarelli and S. Rodriguez , "Recombination of Electrons and Donors in n-Type

- Germanium", *Phys. Rev.*, **124**, 1321 (1961).
12. R.A. Brown and S. Rodriguez , "Low-temperature Recombination of Electrons and Donors on n-Type Germanium and Silicon", *Phys. Rev.*, **153**, 890 (1967).
 13. V.N. Ababkumov, V.I. Perel', and I.N. Yassievitch , "Capture of Carriers by Attractive Centers in Semiconductors", *Sov. Phys. Semicond.*, **12**, 1 (1978).
 - 14 . E.E. Haller, N.P. Palaio, M. Rodder, W.L. Hansen, and E. Kreysa, in *Proc. of 4th Intl. Conf. on Neutron Transmutation Doping of Semiconductors*, R.D. Larabee ed., Plenum Press, 1984
 - 15 . N.P. Palaio, M.S. thesis, Univ. of California, Berkeley, Lawrence Berkeley Laboratory Report LBL-16695, 1983
 - 16 . N.M. Haegel, M.S. Thesis, Univ. of California, Berkeley 1983
 - 17 . B.I. Shklovskii and A.L. Efros 1984 *Electronic Properties of Doped Semiconductors*, Springer-Verlag, New York 1984
 - 18 . E.N. Grossman 1987a, *A Far-infrared Heterodyne Spectrometer for Airborne Astronomy*, Ph. D. dissertation, California Institute of Technology 1987
 - 19 . D.M. Watson, E.N. Grossman, and T.G. Phillips 1988, *in preparation*
 20. H. Krautle, E. Sauter, and G.V. Schultz , "Antenna Characteristics of Whisker Diodes Used as Submillimeter Receivers", *Infrared Physics*, **17**, 477 (1977).
 21. E.N. Grossman , "The Performance of Schottky Diodes as Far-infrared Modulators", *Intl. J. of IR and MM Waves*, **8(10)**, 1293 (1987).
 22. S.W. Teitworth and R.M. Westervelt , "Chaos and Broadband Noise in Extrinsic Photoconductors", *Phys. Rev. Lett.*, **56(5)**, 516 (1984).

Figure Captions

Figure 1 - Block diagram the FIR heterodyne receiver used, in modified form, to measure Ge:Ga bandwidth and photoconductive gain (Watson, Grossman, and Phillips 1988)

Figure 2 - Field dependence of the recombination bandwidth, measured on detector 496-5.5. The rolloff at high field is due to carrier heating.

Figure 3 - Measured recombination bandwidth as a function of minority impurity concentration, for the NTD detectors. The dotted line corresponds to the linear dependence of equation 10, using a carrier temperature of $T_h = 4.2$ K, and a recombination cross-section of $\sigma_r = 3.2 \times 10^{-13} \text{cm}^2$.

Figure 4 - Direct detection responsivity as a function of compensating impurity concentration

Tables

Table 1 - Doping Concentrations of Samples (cm^{-3})

Series	Sample	As grown (P)	NTD		Final	
			N_A	N_D	N_A	N_D
20	496-5.5(20)	$\sim 10^{12}$	3×10^{14}	9.6×10^{13}	3×10^{14}	9.6×10^{13}
	729-6.0(20)	5.0×10^{13}	3×10^{14}	9.6×10^{13}	3×10^{14}	1.4×10^{14}
	729-9.0(20)	8.0×10^{13}	3×10^{14}	9.6×10^{13}	3×10^{14}	1.8×10^{14}
	729-13.0(20)	1.0×10^{14}	3×10^{14}	9.6×10^{13}	3×10^{14}	2.0×10^{14}
21	729-6.4(21)	5.0×10^{13}	6×10^{14}	1.9×10^{14}	6×10^{14}	2.4×10^{14}
	729-9.4(21)	8.0×10^{13}	6×10^{14}	1.9×10^{14}	6×10^{14}	2.7×10^{14}
	729-14.6(21)	1.5×10^{14}	6×10^{14}	1.9×10^{14}	6×10^{14}	3.4×10^{14}
22	729-6.4(22)	5.0×10^{13}	1×10^{15}	3.2×10^{14}	1×10^{15}	3.7×10^{14}
	729-9.4(22)	8.0×10^{13}	1×10^{15}	3.2×10^{14}	1×10^{15}	4.0×10^{14}
	729-14.6(22)	1.5×10^{14}	1×10^{15}	3.2×10^{14}	1×10^{15}	4.7×10^{14}
	729-17.0(22)	2.0×10^{14}	1×10^{15}	3.2×10^{14}	1×10^{15}	5.2×10^{14}

Table 2 - Photoconductive gain derived from g-r noise

Sample	E_{bias} (V/cm)	μ_{Hall} (cm ² /V - s)	$G = \langle i^2 \rangle / 4e i_{DC}$
496-5.5(20)	5.5	-	.021
729-6.0(20)	9.8	2.5×10^4	.032
729-13.0(20)	15	9000	.028
729-9.4(21)	12	6000	.025
729-9.4(22)	18	-	.022
729-14.6(22)	20	-	.015
729-17.0(22)	25	-	.014

LAWRENCE BERKELEY LABORATORY
TECHNICAL INFORMATION DEPARTMENT
UNIVERSITY OF CALIFORNIA
BERKELEY, CALIFORNIA 94720